Journal of Power Sources 626 (2025) 235711

Contents lists available at ScienceDirect

Journal of Power Sources

journal homepage: www.elsevier.com/locate/jpowsour

Effect of ligand variation on Mg alkoxyborate electrolytes: Does more fluorine help?

Tjaša Pavčnik [a,b,c], Muath Radi [c,d], Olivera Lužanin [a,b], Rémi Dedryvère [d,e,f], Deyana S. Tchitchekova [c], Alexandre Ponrouch [c,e], Jan Bitenc [a,b,*], Robert Dominko [a,b,e]

[a] National Institute of Chemistry, Hajdrihova 19, 1000, Ljubljana, Slovenia
[b] Faculty of Chemistry and Chemical Technology, University of Ljubljana, Večna pot 113, 1000, Ljubljana, Slovenia
[c] Institut de Ciència de Materials de Barcelona, ICMAB-CSIC, Campus UAB, 08193, Bellaterra, Spain
[d] IPREM CNRS, Université de Pau & Pays Adour, E2S-UPPA, 64000, Pau, France
[e] Alistore-European Research Institute, CNRS FR 3104, Hub de l'Energie, Rue Baudelocque, 80039, Amiens, France
[f] RS2E, Réseau sur le Stockage Electrochimique de l'Energie, FR CNRS 3459, France

HIGHLIGHTS

- Investigation of the ligand fluorination degree on the performance of Mg alkoxyborate electrolytes.
- Low ionic conductivity and limited dissociation of the electrolyte with least fluorinated ligand.
- Mg plating/stripping efficiency close to 99 % for two best performing electrolytes.
- Beneficial effect of higher amount of boron species in the Mg metal/electrolyte interphase.
- Best organic cathode cycling performance with most fluorinated alkoxyborate electrolyte.

GRAPHICAL ABSTRACT

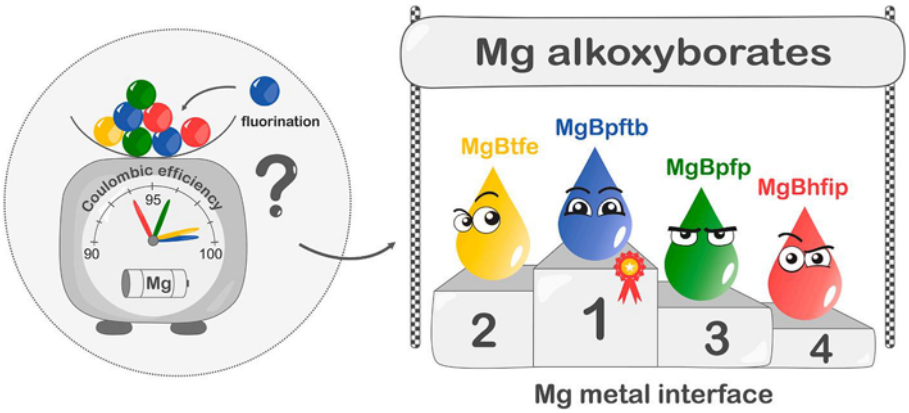

ARTICLE INFO

Keywords:
Mg fluorinated alkoxyborate electrolyte
Ionic conductivity
Plating/stripping
Metal/electrolyte interphase
Organic cathode

ABSTRACT

Mg fluorinated alkoxyborate-based electrolytes are promising candidates for rechargeable Mg batteries. In this work, we investigate a series of Mg alkoxyborates with a different degree of anion fluorination in terms of their physicochemical properties, Mg metal anode, and organic cathode electrochemical performance, as well as Mg metal/electrolyte interphase. The results underscore the significant influence of the anion fluorination degree on the transport properties of electrolytes. Notably, the anion with the lowest degree of fluorination exhibits one order of magnitude lower ionic conductivity than electrolytes with more fluorinated anions. Interestingly, the same electrolyte demonstrates the second-best electrochemical performance, with the Mg plating/stripping efficiency close to 99 %. XPS analysis of the Mg metal deposit surface reveals that the high Coulombic efficiency is associated with a high amount of boron-containing species in the metal/electrolyte interphase of the best-performing electrolytes. Additionally, it has been noted that inorganic boron species result in a larger

* Corresponding author. National Institute of Chemistry, Hajdrihova 19, 1000, Ljubljana, Slovenia.
E-mail address: jan.bitenc@ki.si (J. Bitenc).

https://doi.org/10.1016/j.jpowsour.2024.235711
Received 21 August 2024; Received in revised form 3 October 2024; Accepted 24 October 2024
Available online 6 November 2024
0378-7753/© 2024 The Authors. Published by Elsevier B.V. This is an open access article under the CC BY license (http://creativecommons.org/licenses/by/4.0/).

interfacial resistivity for Mg plating/stripping compared to boron species in an organic environment. Testing in combination with organic cathodes reveals the superior performance of the most fluorinated electrolyte in terms of cycling stability and Coulombic efficiency. The present work underlines the interplay of different phenomena affecting the overall electrochemical performance of electrolytes and strategies for the design of next-generation Mg electrolytes.

1. Introduction

Flexible and scalable electrical energy storage is a key technology in the current energy transition. However, almost exclusive reliance on Li-ion batteries as the go-to energy storage solution is concerning due to their dependency on materials designated as critical raw materials and their increasing price due to surging demand [1]. To establish a sustainable and resilient energy storage landscape, it is essential to explore and develop alternative battery technologies. Multivalent (Mg, Ca, Al) batteries emerge as promising candidates, offering the potential to alleviate resource constraints associated with traditional Li-ion batteries as well as high-energy density due to the high gravimetric and volumetric capacities of metal anodes. Among various multivalent candidates, there is a growing interest in Mg batteries due to the favorable electrochemical properties of Mg metal and the natural abundance of Mg resources. While research focuses on various aspects of Mg batteries, the electrolyte, facilitating the movement of charge carriers and interacting with both electrodes remains the starting point of the Mg battery technology advancement. For practical applications, Mg electrolytes will have to fulfill specific performance benchmarks. To prevent ion-transport limitations the ionic conductivity of electrolytes in a range of the order of mS cm^{-1} is required. Additionally, high anodic stability above 3.0 V *vs.* Mg/Mg^{2+} is needed to facilitate the use of high-voltage cathode materials. To enable long-term cycling with high capacity retention, the Coulombic efficiency of Mg plating/stripping above 99.99 % should be targeted [2]. This can be achieved by designing Mg electrolytes reductively stable against the Mg metal anode or forming a stable, yet Mg^{2+} cation conductive metal/electrolyte interphase. Furthermore, electrolytes should be compatible with various electrode materials (e.g. electrophilic sulfur, transition metal-containing oxides) and non-reactive with common current collectors.

Non-nucleophilic chloride-free electrolytes, specifically, electrolytes based on salts containing weakly coordinating anions (WCA) enable facile dissociation of salts, resulting in improved physicochemical and electrochemical properties of electrolytes to meet the practical performance demands. A specific class of WCA-based electrolytes that have moved into the research spotlight are Mg fluorinated alkoxyborates. Zhao-Karger et al. [3] reported tetrakis(hexafluoroisopropoxy)borate ($Mg[B(hfip)_4]_2$ or MgBhfip), which exhibited promising electrochemical performance, a Coulombic efficiency of Mg plating/stripping up to 98 % and an oxidative stability of 4.3 V *vs.* Mg/Mg^{2+}. This study initiated additional research on MgBhfip including the investigation of the alternative salt synthesis protocols, optimization of electrolyte composition, and its compatibility with different cathode materials [2,4,5]. Additionally, the initial report on the MgBhfip model salt showcased the possibility of tailoring the anion structure by substituting the hfip ligand with alternative fluorinated alkoxy ligands although no electrochemical performance evaluation was disclosed. Later, Liu et al. [6] reported Mg perfluorinated pinacolatoborate ($Mg[B(pfp)_2]_2$ or MgBpfp), which demonstrated high oxidative stability (4.0 V *vs.* Mg/Mg^{2+}), good ionic conductivity (3.95 mS cm^{-1}), and improved Mg plating/stripping compared to the MgBhfip electrolyte [7]. Enhanced properties of the MgBpfp electrolyte were attributed to the chelating effect upon bidentate binding of fluorinated alkoxy groups to the boron central atom and additional stabilization of the anion. Moreover, Ren et al. [8] reported Mg tetrakis(trifluoroethanoxy)borate ($Mg[B(tfe)_4]_2$ or MgBtfe), which demonstrated stable cycling and reversible Mg plating/stripping with a Coulombic efficiency of up to 99 % and overpotentials below 0.2 V.

Mg alkoxyborates have been explored also through computational modeling. Jankowski et al. [9] conducted a broad DFT study on a series of Mg alkoxyborates employing different ligands to examine cation-anion interactions and their correlation to the mechanisms of electrolyte decomposition at the Mg anode surface. Their results suggest that the key to high-performing electrolytes is a balance between the number of electron-withdrawing groups that contribute to high oxidative stability as well as to low interaction energy of the anion, and the degree of ligands' stabilization, which influences the reductive decomposition of the anion. They concluded that the hfip ligand may present the best compromise among investigated alcohols. Additionally, Xie et al. [10] investigated the decomposition kinetics of Mg alkoxyborates and found that the breakage of the B–O bond is governed mainly by steric factors. Although theoretical studies can guide the rational design of novel materials by providing insights into potential candidates with desirable properties, it is important to emphasize that modeling inherently includes certain simplifications, which might overlook effects from linked phenomena on the electrochemical performances. Due to the time and computational cost limitations modeling often neglects or simplifies certain effects like explicit solvent-salt interactions, the effect of surface potential, different crystal lattices on working electrodes, and the effect of impurities, which might play a key role [11]. In addition, the formation of a passivation layer may induce a strong kinetic limitation to electrolyte reduction and/or oxidation, which cannot be considered through modeling. Thus, carefully designed systematic experiments are necessary to complement and validate the findings of computational modeling. Recently, Li et al. reported on a synthesis process of Mg and Ca alkoxyborates and investigated their solvation shell properties and correlations with the electrochemical performance of the corresponding electrolytes. The obtained results again pointed toward MgBhfip as the best-performing Mg salt [12].

With respect to experimental reports on Mg alkoxyborates, they typically focus on one or at most two specific salts, rather than systematically investigating a series of electrolytes with different fluorination degrees. In addition, different salts are typically investigated at different electrolyte concentrations and/or using different solvents, types of electrochemical cells, and cycling protocols. Thus, the properties of electrolytes cannot be directly compared between different reports. Moreover, the salt syntheses differ in starting materials and their purity as well as the protocols for purification of the final products. It is important to note that the synthesis procedure has a large impact on electrochemical performance, as it has been shown for MgBhfip, MgBtfe, and $Mg[Al(hfip)_4]_2$ electrolytes [4,8,13]. Thus, the investigation of a series of electrolytes under comparable conditions is of utmost importance. Among different syntheses reported, the most common and simple approach towards fluorinated Mg alkoxyborates is to use Mg borohydride, in which hydrogen atoms are replaced with the alkoxy groups from the corresponding alcohols. The metathesis reaction is accompanied by hydrogen evolution [3]. However, to the best of our knowledge, a comprehensive investigation spanning from the physicochemical characterization of the electrolyte, Mg metal anode and cathode electrochemical performance, and Mg metal interphase with different fluorinated Mg alkoxyborates synthesized under comparable conditions has not yet been conducted.

In the present work, we aim to address this gap. A series of Mg alkoxyborates with a variable degree of anion fluorination is systematically investigated as Mg electrolytes in diglyme (G2) solvent. Four different Mg electrolytes are synthesized and characterized in terms of

their physicochemical properties, electrochemical performance, and Mg metal/electrolyte interphase composition. While some of their properties are quite similar, the behavior of electrolytes employing different ligands is governed by particular phenomena revealed via in-depth characterization, which provides a direction for the future design of Mg electrolytes and identifies MgBpftb as the most promising electrolyte candidate for full-cell assembly.

2. Experimental

2.1. Salt syntheses and electrolyte preparation

All salt syntheses were performed under an inert atmosphere in an argon-filled glovebox with O_2 and H_2O levels below 0.1 ppm.

Employed alcohols hexafluoroisopropanol (hfip, Apollo Scientific, 99.9 %), trifluoroethanol (tfe, Acros Organics, 99.8 %), perfluoro-tert-butanol (pftb, Apollo Scientific, 98 %), perfluoropinacol (pip, Fluorochem, 98 %) and hexane (Carlo Erba, 95 %) were dried with 4 Å molecular sieves for 4 days before use. 1,2-dimethoxyethane (G1, Sigma-Aldrich, HPLC grade, 99.9 %) and 1-methoxy-2-(2-methoxyethoxy)ethane (diglyme, G2, Acros Organics, 99 %) solvents underwent a three-step drying/purification procedure, including 3 days of drying with 4 Å molecular sieves, reflux upon the Na/K alloy addition and fractional distillation. The amount of water in glyme solvents after the employed procedure was determined by Karl Fischer Coulometric titration, which was found to be < 1 ppm. Acetonitrile (ACN, Sigma Aldrich, 99.9 %) was dried in a similar way, but without the reflux step due to the incompatibility of solvent with the Na/K alloy. The final water content of dried ACN was determined by Karl Fischer titration, which was below 5 ppm.

Mg alkoxyborates, with a general formula $Mg[B(OR^F)_4]_2$ (OR^F = fluorinated alkoxy group), were synthesized from Mg borohydride, $Mg(BH_4)_2$, and selected fluorinated alcohol ($H–OR^F$), by modified reported synthesis procedure for a specific salt, MgBhfip [3]. Briefly, $Mg(BH_4)_2$ was synthesized following the reported procedure [14] and dissolved in G1. $H–OR^F$ alcohol (4.2 eq. of PFP and 8.5 eq. of TFE, HFIP, and PFTB) was dropwise added into the stirred solution. The reaction mixture was stirred for 24 h at room temperature. Afterward, the solvent and residual alcohol were removed under reduced pressure to obtain a concentrated solution. The solution was slowly added into hexane to precipitate $Mg[B(OR^F)_4]_2$ salt. The obtained salt was filtered using a polytetrafluoroethylene (PTFE, pore size 0.22 μm) membrane and dried under vacuum for 48 h at 50 °C. Details on the specific salt synthesis are provided in Supporting Information.

Electrolytes of different concentrations were prepared by weighting the appropriate amount of the selected salt into a measuring flask and diluting it up to the mark with the G2 solvent.

2.2. Characterization of salts

Infrared (IR) spectroscopy measurements were performed under an inert atmosphere on the ATR-IR Alpha II (Bruker) spectrometer equipped with a Ge crystal. All spectra were recorded at room temperature. Measurements were collected and averaged over 48 scans in the range between 3000 and 600 cm^{-1}.

Nuclear magnetic resonance (NMR) spectroscopy measurements (^1H and ^{19}F NMR spectra) were measured on a Bruker AVANCE NEO 600 MHz NMR spectrometer in DMSO-d_6 solvent. Chemical shifts are reported in ppm using the residual solvent peak (in ^1H spectra) and trifluoroacetic acid (in ^{19}F spectra) as a reference. Trifluoroacetic acid was also used as an internal standard to determine the number of G1 molecules coordinated to Mg^{2+} cation in MgBpftb and MgBpfp salts, and the number of fluorine atoms in all salt structures.

2.3. Physicochemical characterization of electrolytes

Ionic conductivities of electrolytes were measured on the FRA-based Multiplexed Conductivity Meter MCM 10 (BioLogic Science Instruments). The conductivity cell was calibrated by measuring the conductivity of the standard solution provided by Mettler Toledo. Electrolytes of different concentrations were measured in a temperature range from 5 to 60 °C with 5 °C steps, allowing for a minimum of 30 min of equilibration time. The viscosity and density of investigated electrolytes were measured in the temperature range from 5 to 60 °C with 5 °C steps on a Lovis 2000 M/ME and a DMA 4500 from Anton Parr. The cell temperature was regulated within ±0.02 °C.

2.4. Electrochemical characterization of electrolytes

Electrochemical measurements were performed in 2- and 3-electrode Swagelok cells. Cells were assembled with three glass fiber separators (Whatman, GF/A, 260 μm) wetted with approximately 100 μL (2-electrode cell) or 200 μL (3-electrode cell) of the selected electrolyte. Mg foil (0.1 mm, Changsha Rich Nonferrous metals, 99.95 %) was polished with P1200 sandpaper before use as a counter electrode (CE). Platinum discs (0.04 mm, Ögussa, 99.99 %) were used as working electrode (WE). In 3-electrode cells, Ag wire (0.05 mm, Goodfellow, 99.99 %) was used as the pseudo-reference electrode (RE). To calibrate the potential of RE, ferrocene (Fc, 10 mM) was introduced into the electrolyte as an internal standard.

Organic cathodes were prepared by mixing organic active material (polyimide polymer, P-NTCDA, synthesis details in Supporting Information), carbon black (Printex XE2), and PTFE binder (Sigma Aldrich, 60 % water dispersion) in a ratio of 60:30:10. The components were dispersed in isopropanol and ball milled on a Retsch PM100 planetary mill at 300 rpm for 30 min. The resulting slurry was further mixed in mortar to obtain a composite. Afterward, the electrode composite was rolled between the glass plate and parchment paper to obtain self-standing electrodes (12 mm) with active material loading between 1.5 and 2.0 mg cm^{-2}.

Electrochemical measurements were performed on a VMP3 potentiostat from Bio-Logic S. A. Galvanostatic cycling included Mg plating with a current density of 1 mA cm^{-2} for 1 h (1 mAh cm^{-2}) and stripping to a cut-off voltage of 2.0 V. Rate capability experiments were performed by Mg plating/stripping at current densities of 0.1, 0.2, 0.5, and 1.0 mA cm^{-2} (1 mAh cm^{-2}), for 10 cycles at each current density. Linear sweep voltammetry (LSV) was performed by scanning the potentials from open circuit voltage (OCV) to 3.0 V *vs.* Ag wire (RE) at a 0.01 mV s^{-1} rate. The stability of the electrolytes is reported as potential at which a current density of 0.9 μA cm^{-2} was reached. To ensure the reproducibility of the results, all electrochemical measurements were conducted in three parallel cells. The reported comparisons (absolute differences) among different data sets refer to the plotted data, which represent the median values of the three parallel cells. The tested cells have high reproducibility with the standard deviation within a few %.

Organic active materials were tested in a 2-electrode cell with Mg metal anode as a counter electrode using a C-rate of C/2, calculated per amount of organic active material.

2.5. Characterization of Mg deposits - XPS

Samples for XPS characterization were prepared in 2-electrode Swagelok cells, where the Pt working electrode was replaced with carbon-coated Al foil to improve the adhesion of Mg deposits. In these cells, an additional Celgard separator was added on top of the glass fiber separator to avoid contamination of the electrode surface by glass fibers. Cells underwent galvanostatic cycling at 1 mA cm^{-2} (1 mAh cm^{-2}) with an upper potential limit of 2.0 V, for 10.5 cycles, ending with Mg plating on the carbon-coated Al foil substrate. Afterward, cells were transferred to the glovebox and disassembled. Substrates with collected deposits

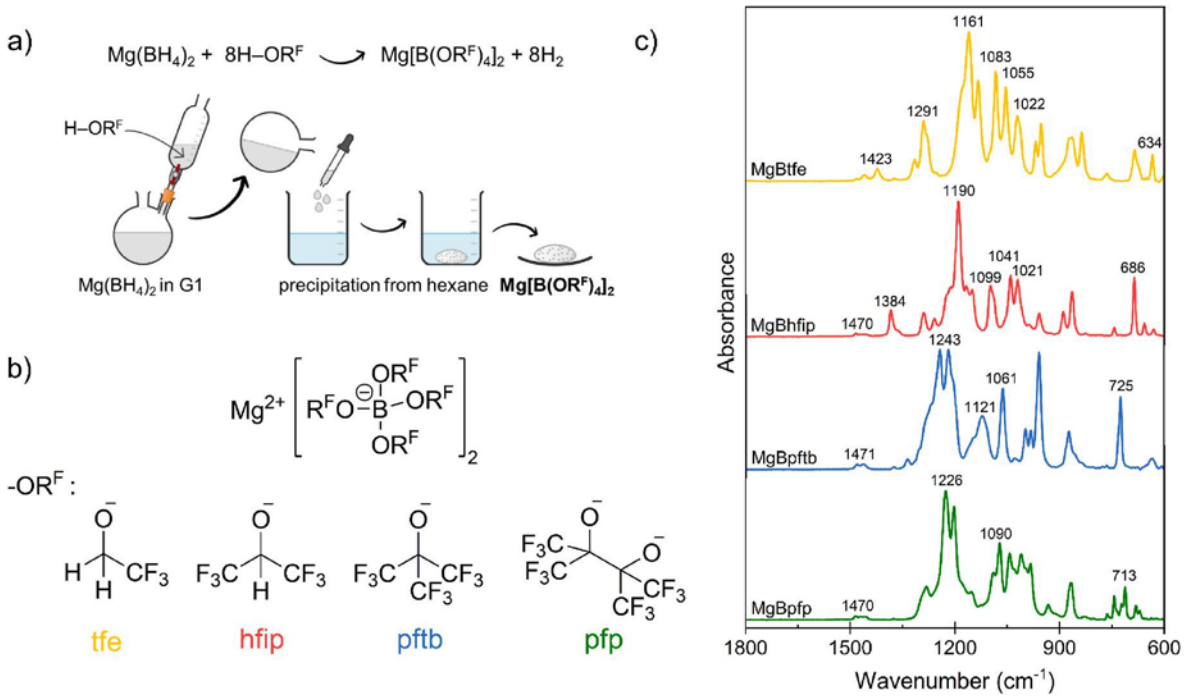

Fig. 1. a) Schematic of a general synthesis procedure of Mg alkoxyborates; **b)** General structure of Mg alkoxyborates and selected ligands (–OR^F). Note that the pfp ligand is bidentate and binds as $Mg[B(pfp)_2]_2$; **c)** IR spectra of Mg alkoxyborates with marked characteristic peaks.

were rinsed with G2 solvent to wash the remaining electrolyte, dried, and under an inert atmosphere transferred to the XPS instrument.

The Thermo Scientific ESCALAB 250 spectrometer with a focused monochromatized Al Kα radiation ($h\nu$ = 1486.6 eV) was used to accomplish the XPS measurements. The core level peaks were recorded with a pass energy of 20 eV and 600 μm spot size at a pressure of around 2×10^{-7} mbar in the analysis chamber pressure and by using the standard charge compensation. The binding energy scale was calibrated using the C 1 s peak at 285 eV associated with adventitious hydrocarbon. The analyses were performed on at least two different points for each sample to have representative measurements of the surface (*i.e.* to check the surface homogeneity). The data were fitted and analyzed using CasaXPS software with the relative sensitivity factor (RSF) of the ESCALAB database.

2.5.1. The assignation of boron species

Since different kinds of boron in an oxygen environment have similar binding energies, the assignation of boron species was done with the support of quantitative data. To do so, we started from the amount of oxygen corresponding to the O 1s peak at ≈532.5 eV (*i.e.*, not attributed to MgO), and we subtracted the amount of oxygen corresponding to the salt and organic CO, CO_2, and CO_3 environments. If any, the remaining oxygen was then attributed to inorganic boron B_xO_y, which is the only remaining source of oxygen. Analysis of different points of the same sample showed that a constant B/O ratio equal to ~1.5 was observed for this inorganic boron. Therefore, we attributed this inorganic boron (B_2O_3 or similar B–O species). The boron that was not attributed to the latter was then considered as linked to organic CO and CO_2 environments.

2.6. DFT calculation of alkoxyborate anion structures

DFT calculations of the alkoxyborate anions were performed with ORCA 5.0.3 package [15] using the BP86 functional with Grimme's D3 empirical dispersion correction and def2-TZVPD basis set, designed to provide consistent accuracy across the entire periodic table [16]. The as optimized geometries were confirmed as energy minima from the computed vibrational frequencies (absence of imaginary frequencies) at the same level of theory.

3. Results and discussion

Mg alkoxyborates can be synthesized through various methods: metathesis reaction between $Na[B(OR^F)_4]$ and $MgBr_2$ [3], trans-metalation reaction between Mg and B-based sources [4], or a one-pot reaction from $Mg(BH_4)_2$ and the selected alcohol [3]. Among them, we selected the latter as our preferred synthesis approach due to the availability of reactants and its time and cost efficiency. Additionally, by employing the selected synthesis procedure for all the investigated salts, we reduced the number of different synthesis steps for each ligand. A general procedure (Fig. 1a) was adopted from the literature [3] with a modification in the salt isolation step, where salt is precipitated from hexane. The latter contributes to obtaining Mg salts with a higher purity [13]. Different ligands (-OR^F) used for the synthesis of salts are shown in Fig. 1b. Selected ligands vary in the degree of fluorination, listed in increasing order: 2,2,2-trifluoroethanoxy (tfe), 1,1,1,3,3,3-hexafluoroisopropoxy (hfip), perfluorotertbutanoxy (pftb), with one to three $–CF_3$ groups, respectively. The fourth ligand is perfluoropinacolato (pfp), which is similar to hfip but has two donor oxygens resulting in bidentate binding to the boron central atom and elimination of α-proton. Details on the synthesis of the specific salt are provided in the Experimental and Supporting Information.

IR spectra of synthesized salts are shown in Fig. 1c. Strong peaks at 1161, 1190, 1243, and 1226 cm^{-1} for MgBtfe, MgBhfip, MgBpftb, and MgBpfp, respectively, are attributed to the B–O–C stretching vibrations and $–CF_3$ symmetric and antisymmetric stretching vibrations. The deformation mode of the $–CF_3$ group results in medium-intensity peaks at 634, 686, 725, and 713 cm^{-1} for the salts listed in the aforementioned order, while deformations of the O-B-O bonds appear at lower wavenumbers around 600-650 cm^{-1}, visible in the low-intensity peaks in this region of MgBhfip, MgBpftb, and MgBpfp, respectively. Peaks in the range of 1021–1121 cm^{-1} correspond to C–O stretching vibrations [17]. In the spectra of MgBhfip, MgBpftb, and MgBpfp, a low-intensity broad peak at 1471 cm^{-1} represents the C–H deformation of methyl and

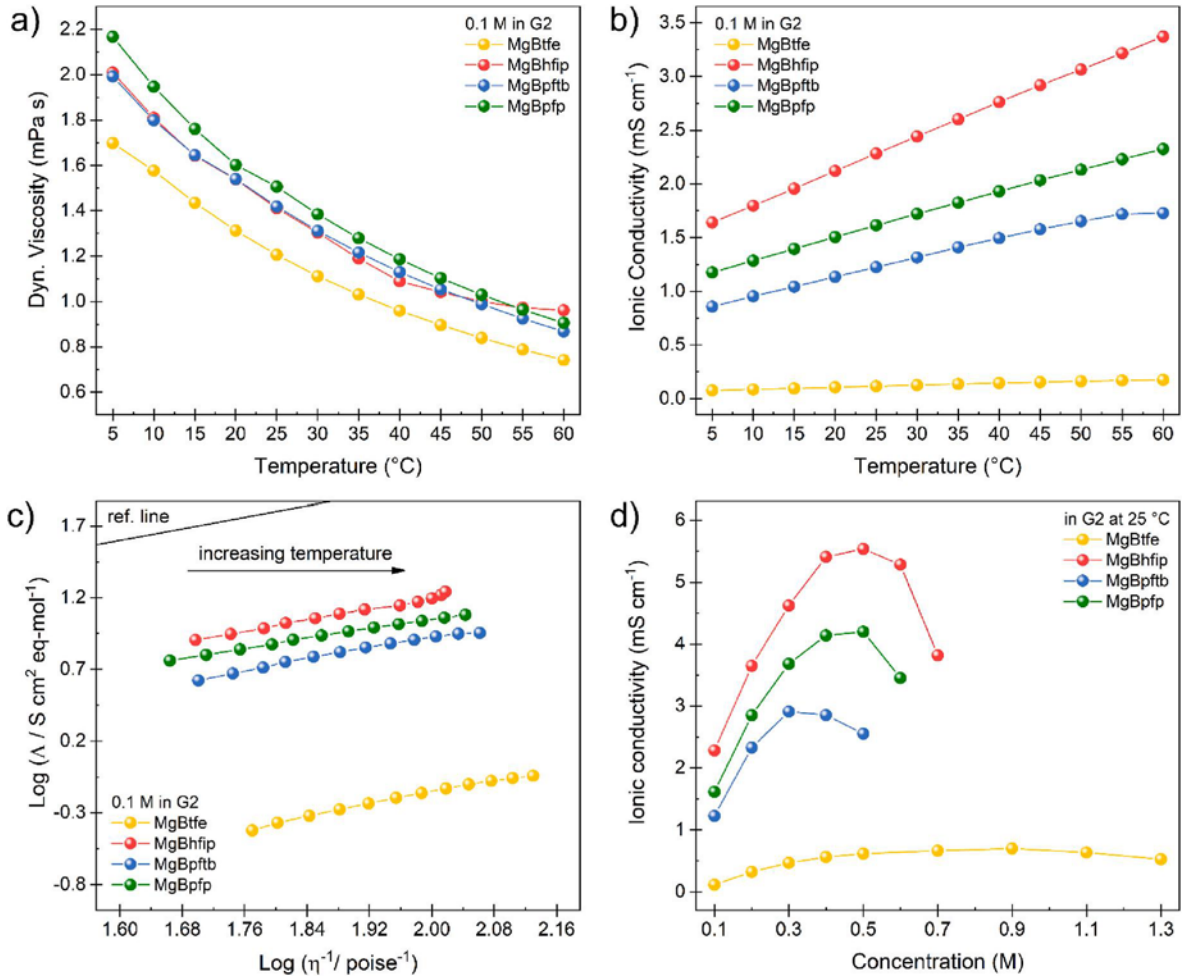

Fig. 2. Physicochemical characterization of Mg alkoxyborates in G2. **a)** Dynamic viscosity of 0.1 M electrolytes at different temperatures; **b)** Ionic conductivity of 0.1 M electrolytes at different temperatures; **c)** Walden plot of 0.1 M electrolytes at different temperatures; **d)** Ionic conductivity of electrolytes at different concentrations at 25 °C.

methylene groups, indicating the coordination of G1 molecules to the Mg cation, consistent with the literature reports [18,9]. In the spectrum of MgBtfe, this peak appears at 1423 cm^{-1}. The observed shift is attributed to the difference in salt structure between the MgBtfe and other salts, resulting in different vibrational environments of the Mg^{2+}-G1 complexes. One can note additional peaks are shifted depending on the anion fluorination of measured salt. The presence of electron-withdrawing $–CF_3$ groups tends to decrease the electron density in B–O–C and C–O bonds, resulting in blue-shifted peaks. Notably, peaks of the $Btfe^-$ anion (the least fluorinated among studied anions), appear at a lower wavenumber compared to peaks of the $Bhfip^-$ anion (moderate degree of fluorination), and the perfluorinated $Bpftb^-$ and $Bpfp^-$ anions. The peak positions and their shifts upon increased fluorination degrees were confirmed by the DFT-computed frequencies and IR intensities of the studied anions (Fig. S1 and Table S1), which demonstrate a strong correlation with the experimental data. Notably, the IR spectra of all synthesized salts do not show the characteristic peak of $Mg(BH_4)_2$ at 2268 cm^{-1} (Fig. S2), confirming the complete conversion of the reagent.

Syntheses of salts have been performed in the G1 solvent, which is incorporated into the crystal structure of salts [3]. Thus, the ^1H NMR spectra of the measured salts (Fig. S2a) show peaks at 3.42 and 3.23 ppm corresponding to the $–CH_2–$ and $–CH_3$ protons from G1 molecules coordinated to the Mg^{2+} cation. For MgBhfip, MgBpftb, and MgBpfp salts, the $–CH_2–$ and $–CH_3$ peaks integrate for 12 and 18 protons, respectively, suggesting the coordination of three G1 molecules. A specific difference is observed in the case of MgBtfe, where peaks for G1 integrate for 4 and 6 protons, indicating the coordination of only one G1 molecule. The distinct structure of MgBtfe is attributed to the less pronounced WCA character of the $Btfe^-$ anion and a stronger tendency for cation-anion interactions in this salt. The proximity of the anion to the Mg^{2+} cation hinders the coordination of additional G1 molecules. Note that the number of G1 molecules in MgBtfe and MgBhfip salts was determined based on the ratio of integrals for the anion and G1 peaks. In the case of perfluorinated anions ($Bpftb^-$, $Bpfp^-$) with no protons in their structure, an internal standard was employed. Additionally, the MgBtfe salt shows a quartet at 3.66 ppm ($^4J = 10.1$ Hz) corresponding to the $–CH_2–$ protons from the $Btfe^-$ anion [8]. Protons from the $Bhfip^-$ anion exhibit a broad multiplet at 4.64 ppm. The trend in the chemical shift for protons in $Btfe^-$ and $Bhfip^-$ anions can be explained by the electronegativity of the atoms, in the vicinity of the atom of interest. Protons in the $Bhfip^-$ anion have a high chemical shift due to the larger number of electron-withdrawing $–CF_3$ groups compared to the $Btfe^-$ anion. The reduced electron density of protons in the $Bhfip^-$ anion decreases the shielding and increases the resonance frequency.

In ^{19}F spectra, peaks are observed at −74.23, −74.25, −70.74, and −69.26 ppm for MgBtfe, MgBhfip, MgBpftb, and MgBpfp salts, respectively (Fig. S2b). Due to the H–F coupling, the signal in the ^{19}F spectrum of the $Btfe^-$ anion appears as a triplet ($^3J = 10.1$ Hz, same coupling constant as in the corresponding ^1H spectrum), and the signal for the H–F coupled atoms in the $Bhfip^-$ anion as a doublet ($^2J = 3.6$ Hz). The signals in the spectra of perfluorinated salts appear as sharp singlets. By introducing an internal standard, the number of fluorine atoms in the

measured salts was determined as 24 fluorine atoms in the $Btfe^-$ anion, 48 F in $Bhfip^-$ and $Bpfp^-$ anions, and 72 F in the $Bpftb^-$ anion. Based on the NMR measurements, salt structures can be predicted as $[Mg(G1)][B(tfe)_4]_2$, $[Mg(G1)_3][B(hfip)_4]_2$, $[Mg(G1)_3][B(pftb)_4]_2$, and $[Mg(G1)_3][B(pfp)_2]_2$. The absence of peaks corresponding to the starting alcohols or any unresolved impurities in the ^1H and ^{19}F spectra confirms the purity of the synthesized salts and efficient synthesis reaction.

3.1. Physicochemical properties

The physicochemical properties of 0.1 M Mg alkoxyborate electrolytes in G2 were measured at temperatures ranging from 5 to 60 °C. The G2 solvent was selected based on previous reports of favorable electrochemical performance over other glymes [2,19]. Measurements demonstrated the following trends: i) density (Fig. S4) decreases with the temperature, as expected due to the volumetric expansion of the liquid, ii) viscosity (Fig. 2a) decreases with the temperature, as the thermal energy becomes sufficient to overcome the intermolecular interactions, and iii) ionic conductivity (Fig. 2b) of electrolytes increases with the temperature due to decreased viscosity, resulting in higher mobility of species. Notably, the electrolyte with the least fluorinated $Btfe^-$ anion exhibits the lowest values of all three measured properties. The most significant difference is observed in ionic conductivity – the MgBtfe electrolyte shows one order of magnitude lower conductivity (0.1 mS cm^{-1} at 25 °C) compared to other investigated electrolytes. Specifically, at room temperature (25 °C), ionic conductivities of 0.1 M MgBhfip, MgBpftb, and MgBpfp electrolytes are 2.3, 1.2, and 1.6 mS cm^{-1}, respectively, at comparable viscosities (≈1.5 mPa s).

Walden plot of 0.1 M Mg alkoxyborate electrolytes is shown in Fig. 2c. Data points of all investigated electrolytes fall below the reference aqueous KCl solution line, indicating that at least to a certain degree ion motion is hindered by ion pairing rather than viscosity. The deviation is again more notable in the MgBtfe electrolyte, showing the lowest ionicity. A slight modification of the curve's slope can be observed at temperatures above 55 °C. This phenomenon is typically observed in low permittivity solvents (such as ethers) and is attributed to temperature-dependent ion pair formation [20].

The electrolytes' physicochemical properties measured can be partially rationalized considering the size of the anions and the resulting degree of charge delocalization and mobility. From DFT calculations (Fig. S1) $Btfe^-$, $Bhfip^-$, $Bpftb^-$, and $Bpfp^-$ fit within spheres with volumes of 255, 375, 495, and 353 $Å^3$, respectively. The smaller anion size and the fewer electron-withdrawing $–CF_3$ groups in $Btfe^-$ compared with the other anions result in a stronger tendency to ion pair formation and thus lower overall ionic conductivity due to the lower amount of free charge carriers, while larger anions ($Bhfip^-$, $Bpftb^-$ and $Bpfp^-$) with more $–CF_3$ groups than $Btfe^-$ are less prone to ion pair formation. Significantly larger anions such as $Bpftb^-$ present lower mobility in solution (inversely proportional to the ion size), hence, the lower overall ionic conductivity at similar salt concentration and temperature pointing at the anions to be the most mobile ionic species in the electrolyte. Therefore, significantly lower total ionic conductivity recorded for MgBpftb-based electrolytes could indicate a higher cation transference number, with well-dissociated cations expected to retain similar mobility regardless of the nature of the anion. For MgBtfe, the high degree of ion pairs results in a lower concentration of free anions in the solution, confirmed by a drastic drop in ionic conductivity observed for MgBtfe-based electrolytes. However, since monovalent Mg-anion ion pairs remain mobile cationic species, a higher cationic transference number can be expected. By contrast, electrolytes based on MgBhfip and MgBpfp salts present the highest ionic conductivities with an optimal compromise between salt dissociation and anion mobility. These results are in agreement with a previous report from Jankowski et al. [9] on the interaction energies ($E_{intr.}$) between cation and anion for the investigated salts following the order: $Btfe^- > Bhfip^- > Bpfp^- > Bpftb^-$.

Ionic conductivity measurements as a function of the electrolyte's concentration show a parabolic shape (Fig. 2d), which is typically observed due to the competition between the increasing number of charge carriers (dominant at low concentrations) and the increase in the viscosity and ion interactions (dominant at high concentrations) [21]. Maximum ionic conductivities of MgBtfe, MgBhfip, MgBpftb, and MgBpfp electrolytes at room temperature (25 °C) are 0.7 mS cm^{-1} (0.9 M), 5.5 mS cm^{-1} (0.5 M), 2.9 mS cm^{-1} (0.3 M), and 4.2 mS cm^{-1} (0.5 M), respectively (Table 1). Notably, the MgBtfe electrolyte stands out with its maximum ionic conductivity observed at the highest salt concentration among investigated electrolytes. By increasing the temperature, the maximum ionic conductivity in MgBtfe, MgBhfip, and MgBpfp electrolytes shifts to higher salt concentrations (Fig. S5), corresponding to the decrease in viscosity (Fig. S6). For example, at 5 °C the maximum ionic conductivity in MgBhfip electrolyte is at 0.4 M, while at 60 °C, it shifts to 0.5 M. In the MgBpftb electrolyte, this is not the case, which may be due to its lower viscosity at higher concentrations compared to other electrolytes.

Table 1
Maximum ionic conductivity of Mg alkoxyborates in G2 and viscosity of electrolytes at the corresponding concentration measured at 25 °C.

Electrolyte	Maximum ionic conductivity		
	Concentration [M]	Ionic conductivity [mS cm^{-1}]	Viscosity [mPa s]
MgBtfe	0.9	0.7	4.0
MgBhfip	0.5	5.5	3.4
MgBpftb	0.3	2.9	1.9
MgBpfp	0.5	4.2	4.7

3.2. Electrochemical performance

The electrochemical performance of 0.4 M Mg alkoxyborate electrolytes in G2 was investigated through galvanostatic cycling at 1 mA cm^{-2} current density in a 2-electrode Swagelok cell setup using a Mg counter and Pt working electrode. The specific concentration of 0.4 M was selected as it offers a good compromise between a low degree of ion pair formation (in MgBhfip, MgBpftb, and MgBpfp, salt-to-G2-solvent ratios are displayed in Table S2) and high ionic conductivity, which is close to the maximum ionic conductivity of each electrolyte (Table S3). The average Coulombic efficiencies of Mg plating/stripping over 20 cycles are 98.6, 93.9, 98.9, and 96.0 % for MgBtfe, MgBhfip, MgBpftb, and MgBpfp electrolytes, respectively (Fig. 3a). The best-performing electrolytes are MgBtfe and MgBpftb, which also show fewer activation cycles, and have high Coulombic efficiency close to 95 % already in the first cycle, while Coulombic efficiencies of first cycles in MgBhfip and MgBpfp electrolytes are significantly lower – 58.3 and 77.6 %, respectively. We tentatively ascribe the higher Coulombic efficiency recorded with MgBtfe and MgBpftb electrolytes to a more stable Mg metal/electrolyte interphase (see section Interphase characterization), as well as potentially higher cation transference number when compared with MgBhfip and MgBpfp with high salt dissociation and high mobility of anions. Interestingly, the former two electrolytes demonstrate significantly higher overpotentials over the latter two. Since a 2-electrode cell setup was used, the recorded overpotentials include contributions from both working and counter electrodes. After the activation in initial cycles, the overpotentials in MgBtfe and MgBpftb electrolytes are approximately 0.2 V, which is more than twice the one recorded in MgBhfip and MgBpfp electrolytes (around 0.07 V, Fig. 3b and S7). Large overpotentials can originate from the Mg metal anode interface or resistance of the bulk electrolyte.

Rate capability experiments were performed and show that decreasing the current density to 0.1 mA cm^{-2} leads to significantly lower overpotentials of 0.07 V and 0.11 V, for MgBtfe and MgBpftb electrolytes (Figs. 3c and S8), respectively. By contrast, in MgBhfip and MgBpfp electrolytes, comparable overpotentials were observed at

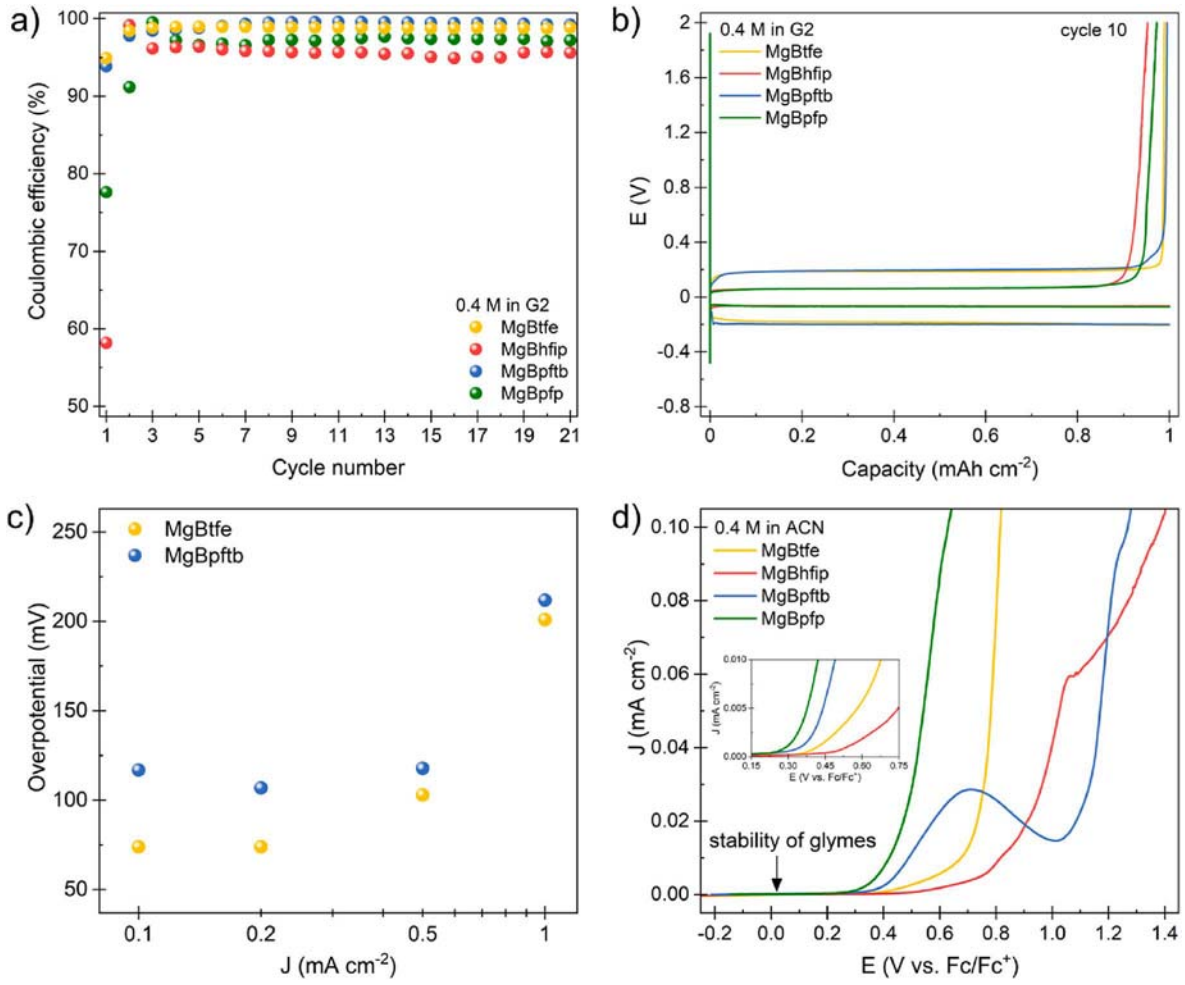

Fig. 3. Electrochemical characterization of 0.4 M Mg alkoxyborates. **a)** Coulombic efficiency of Mg plating/stripping on Pt working electrode at 1 mA cm^{-2} (1 mAh cm^{-2}); **b)** Corresponding galvanostatic curves for the 10th cycle of Mg plating/stripping; **c)** Comparison of overpotentials in MgBtfe and MgBpftb electrolytes at different current densities; **d)** Linear sweep voltammetry of Mg alkoxyborate salts in ACN solvent at a sweep rate 0.01 mV s^{-1}.

different current densities (Table S4, Figs. S9 and S10). Considering the applied current density, electrolyte conductivity, and the distance between the electrodes, the estimated electrolyte resistance contribution to total overpotentials is 70 % in MgBtfe and 14 % in MgBpftb electrolyte (Table S5). This indicates that large overpotentials in the MgBtfe electrolyte mainly originate from the low ionic conductivity of the electrolyte, whereas in the MgBpftb electrolyte, electrolyte resistance is not the main contributor to the cell overpotentials. Rate capability experiments additionally support this, as by decreasing the current density of Mg plating/stripping, the overpotentials decrease by 70 % in MgBtfe and only 40 % in MgBpftb electrolyte (Fig. 3c). The overpotentials in MgBhfip and MgBpfp electrolytes hardly change in the rate capability experiment (Fig. S10), which agrees with relatively low electrolyte resistance contribution in cell overpotentials (20–25 %) and the key role of interfacial resistance.

Electrochemical characterization shows that promising physicochemical properties of electrolyte do not directly translate to the best electrochemical performance, as the MgBtfe electrolyte, despite its poor ionic conductivity, demonstrates Mg plating/stripping with fewer activation cycles and a stable performance with the second-best Coulombic efficiency among investigated electrolytes. On the other hand, the MgBhfip electrolyte, which displays the most promising physicochemical properties, exhibits inferior performance compared with the other electrolytes. Note, that experiments were conducted at 1 mA cm^{-2}, a current density considered moderately high for Mg electrolytes. Nevertheless, the current density may not be sufficiently high to expose the electrolyte's ionic conductivity as a limiting effect on the electrochemical performance, especially given the key role of interfacial processes at the Mg metal anode. To establish an improved understanding of transport phenomena, additional experiments are imperative where the effects of the cation solvation structure, and specific ion mobility have to be studied.

The oxidative stability of Mg alkoxyborate salts was examined through the linear sweep voltammetry (LSV) at a slow scan rate of 0.01 mV s^{-1} in a 3-electrode Swagelok cell with an Ag pseudo-reference electrode. Glyme-type solvents have limited oxidative stability of 3.0 V *vs.* Mg^{2+}/Mg [22], thus, to determine the oxidative stability of salts, measurements were performed in acetonitrile (ACN) solvent with higher oxidative stability, above 5 V *vs.* Li^{+}/Li (corresponding to approximately 2.0 V *vs.* Fc^{+}/Fc) [23]. The determined oxidative stabilities of MgBtfe, MgBhfip, MgBpftb, and MgBpfp electrolytes are 0.41, 0.53, 0.34, and 0.28 V *vs.* Fc^{+}/Fc, respectively (Fig. 3d). In the MgBpftb electrolyte, an oxidation peak was observed before the electrolyte oxidation front and is attributed to electrode passivation. This behavior was found to be fully reproducible. Reported HOMO and LUMO energies, which are commonly used for the estimation of redox properties of species, predict that a higher degree of anion fluorination results in lower energy of HOMO orbital (Table S6) corresponding to higher oxidative stability of the anion, also reported in the literature [10,9]. However, the obtained experimental results do not follow the computationally predicted trend from HOMO orbital calculations, as both perfluorinated anions exhibit lower oxidative stabilities compared to the least fluorinated Btfe. The

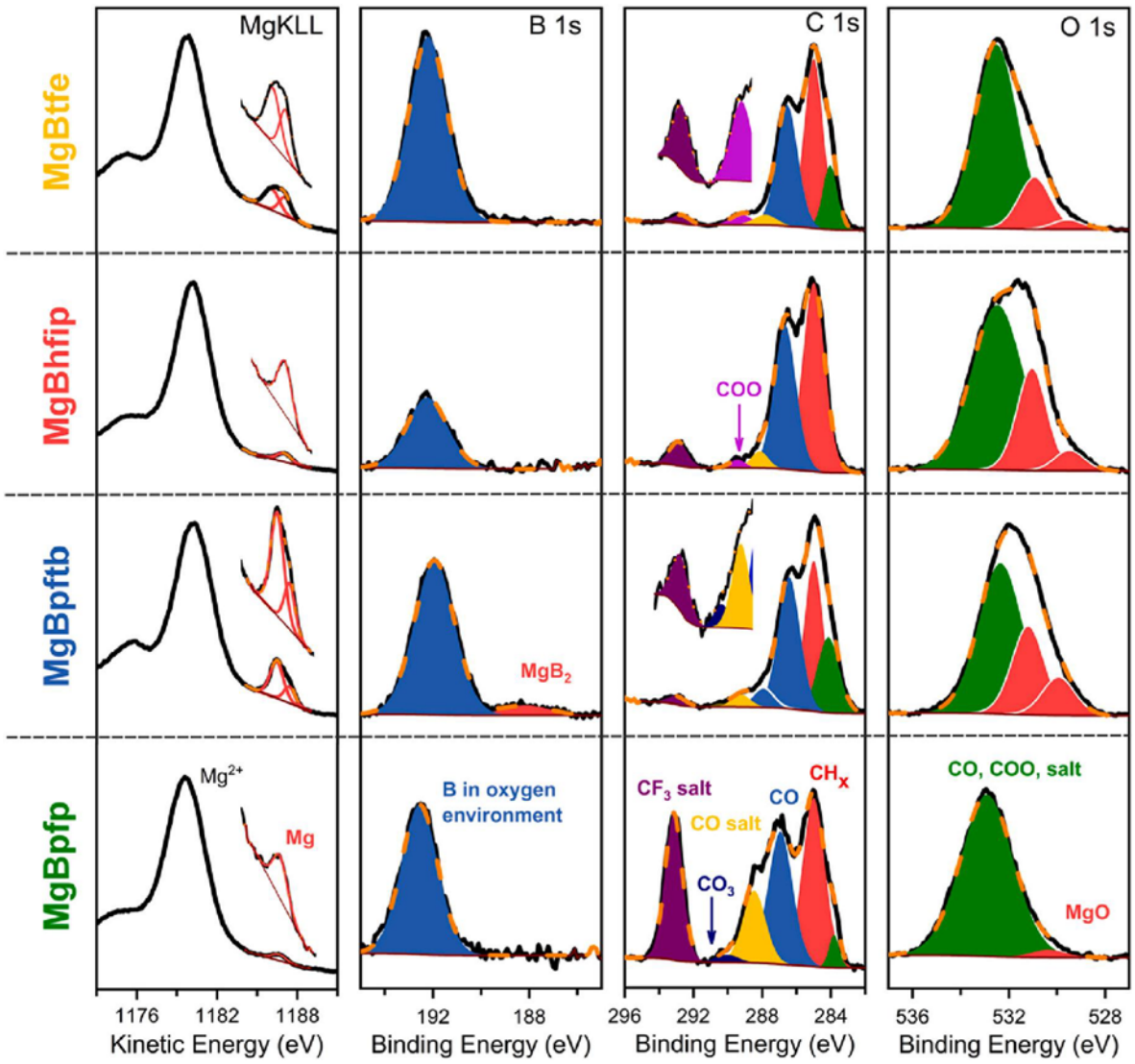

Fig. 4. Auger Mg KLL, XPS B 1s, C 1s and O 1s spectra of the Mg deposits on carbon-coated Al foil substrate in 0.4 M Mg alkoxyborates in G2. The solid and dashed lines represent the measured and fitted data, respectively.

surprisingly good oxidative stability of $Btfe^-$ is likely observed due to the presence of ion pairs in this electrolyte, which tends to shift both HOMO and LUMO energy levels in the negative direction [8], resulting in improved oxidative stability but decreased reductive stability. The $Bhfip^-$ with a moderate degree of anion fluorination was surprisingly identified as the anion with the highest oxidative stability. As mentioned, computational analysis usually focuses only on the stability of bare anions in bulk, while the effects of solvation, ion pairing as well as potential and electrode surface are typically excluded, which can lead to inconsistencies between theoretical and experimental results. Overall, the oxidative stabilities of all investigated Mg alkoxyborate salts are similar and exceed the stability of glyme solvents, which remains the key limitation in the stability of Mg electrolytes.

3.3. Interphase characterization

To better understand the Mg plating/stripping process and interphases formed as well as to complement physicochemical and electrochemical characterization, we investigated the surface of Mg metal deposits with XPS. Mg deposits were prepared on Al carbon-coated working electrodes instead of Pt metal due to poor adhesion of the deposits on Pt foil. The electrochemical characterization does not reveal any significant difference between the two plating substrates (Fig. S11). B 1s, C 1s, and O 1s XPS core peaks and Mg KLL Auger spectra of the Mg deposits are displayed in Fig. 4. Additionally, Mg 2p and F 1s spectra are given in Fig. S12. The results of XPS quantitative analysis are summarized in Table S7 and Chart S1.

The detection of metallic Mg in the Mg KLL Auger spectra clearly confirms the Mg plating process in all investigated electrolytes. Due to the large kinetic energy difference between the signal of Mg^{2+} species and the signal of the Mg metal (~6–7 eV), the detection of metallic deposition is unambiguous. The presence of the metal is additionally confirmed in the Mg 2p spectra (Fig. S12). For MgBpftb and MgBtfe salts, two different peaks for the metallic signal are noted. As detailed in the Supplementary information (Fig. S13), this is due to the separation of small metallic Mg particles from the rest of the metal deposits when the cell is dismantled. Note that the samples showing two signals for the metal also contain a higher quantity of metallic Mg at the surface.

C 1s spectra display various kinds of carbon environments at the sample surfaces, including adventitious hydrocarbon (≈285 eV), carbon in a C–O environment from the solvent at 286.5 eV, C–O environment from the salt (with binding energy varying by neighboring CF_3 groups), C=O (≈288 eV) and O–C=O (≈289 eV) environments. In MgBpftb and MgBpfp samples, a small quantity of carbonate is also observed and

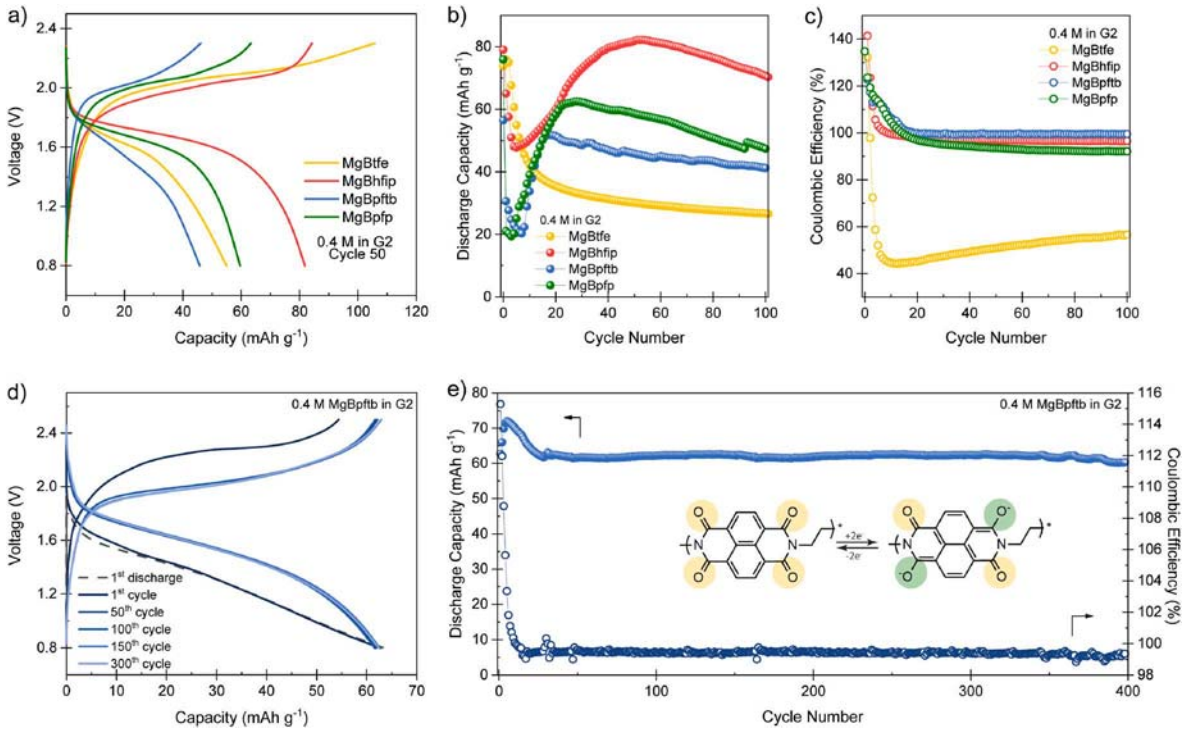

Fig. 5. Electrochemical characterization of Mg metal-organic cathode (P-NTCDA) cells at C/2 current density. **a)** Characteristic galvanostatic cycle for all four alkoxyborate electrolytes in voltage window from 0.8 to 2.3 V, 50th cycle is visualized, except in case of MgBtfe where 5th cycle is displayed due to rapid capacity fade; **b)** Discharge capacity and **c)** Coulombic efficiency *vs.* cycle number in the same voltage window; **d)** Galvanostatic cycles of Mg metal-organic cathode in MgBpftb electrolyte in extended voltage window from 0.8 to 2.5 V and **e)** Corresponding discharge capacity and Coulombic efficiency of the same cell.

attributed to $MgCO_3$. A low binding energy component at ≈284 eV is observed in three of the four samples, and attributed to carbon coating on the substrate.

O 1s spectra show several components. The main peak at approximately 532.5 eV is attributed to various oxygen environments, including the ones from the salt and other oxygenated species at the surface, such as organic CO and COO, as well as inorganic borates. According to the database reference, two lower binding energy components at ≈531 eV and ≈529.7 eV could be attributed to $Mg(OH)_2$ and MgO, respectively [24]. However, the measured O/Mg ratios, as well as additional experiments presented in Fig. S14 (and Table S8), indicate that both signals correspond to MgO, which can be explained by the differential charging effect of a very thin layer of MgO in electrical contact with the metallic Mg (extended explanation in the comment of Fig. S14). The largest quantity of MgO is observed at the surface of the MgBpftb sample (≈28 at%), while 18 at%, 11 at%, and 1 at% of MgO are present in MgBhfip, MgBtfe, and MgBpfp samples, respectively (see Chart S1).

In all samples, the B 1s spectrum displays a peak between 191.9 and 192.6 eV, which corresponds to boron in an oxygen environment (*i.e.* from salt or inorganic/organic borate compounds formed after salt degradation at the surface). For the MgBpftb sample, there is an additional weak peak at 188 eV that cannot be assigned to boron in an oxygen environment. The specific binding energy is typically associated with metal borides [24], thus we assign it to the formation of MgB_2, which is the most probable MgB_x compound resulting from the reduction of the anion at the Mg surface. The reason why this component is not observed in other samples is unclear. According to the quantitative analysis (see Table S7), most of the borate signal does not correspond to the salt, except for the MgBpfp sample, which contains over 50 at% of salt on its surface (as confirmed by the high intensity of the CF_3 component in its C 1s spectrum). The borate signal in MgBtfe, MgBhfip, and MgBpftb mainly corresponds to inorganic and/or organic borate compounds ensuing from salt degradation. Notably, the samples with the highest quantity of boron at the surface exhibit the highest Coulombic efficiency. Since different types of boron in an oxygen environment have similar binding energies, the assignation of boron species was done through quantification and species assignation (details are provided in the Supporting Information). The results of the analysis indicate that the MgBtfe sample mostly contains B–O–C-like (organic) boron, while the MgBpftb sample mostly contains boron in an inorganic environment (B_2O_3 or similar B–O species). The specific interphase composition with a high content of boron-based inorganic species in MgBpftb electrolyte likely contributes to its high Coulombic efficiency but also results in increased overpotentials due to the higher resistance of the formed layer. On the other hand, MgBtfe features a high content of boron in an organic environment, which suggests that such interphase can also prevent further electrolyte decomposition while favoring Mg deposition with good Coulombic efficiency and lower overpotential. As previously reported on the Ca system, boron-containing species in an organic environment can contribute to the formation of a stable passive layer, facilitating reversible electrochemical performance [25]. The MgBhfip sample contains a mixture of both types of boron. In the MgBpfp sample, the surface deposits contain a substantial amount of salt preventing the accurate analysis of residues. Since all samples for XPS measurements were extensively rinsed with the G2 solvent and multiple sites were analyzed, MgBpfp salt seems to be an integral part of the formed interphase rather than the result of poor electrode rinsing. A lower degree of the $Bpfp^-$ anion decomposition compared to the other electrolytes is attributed to the specific anion structure with a strong bidentate binding of ligands to the boron central atom.

All samples show the formation of 2–3 at% of MgF_2 (Fig. S12) as the result of salt degradation at the surface, with less MgF_2 observed in MgBpfp since its contribution is dominated by the salt signal. Additionally, all Mg deposits contain some $MgCl_2$ contamination from the synthesis of the $Mg(BH_4)_2$ precursor. However, a recent study on hfip-based WCA electrolytes showed that small amounts of $MgCl_2$ do not affect the electrochemical performance [2].

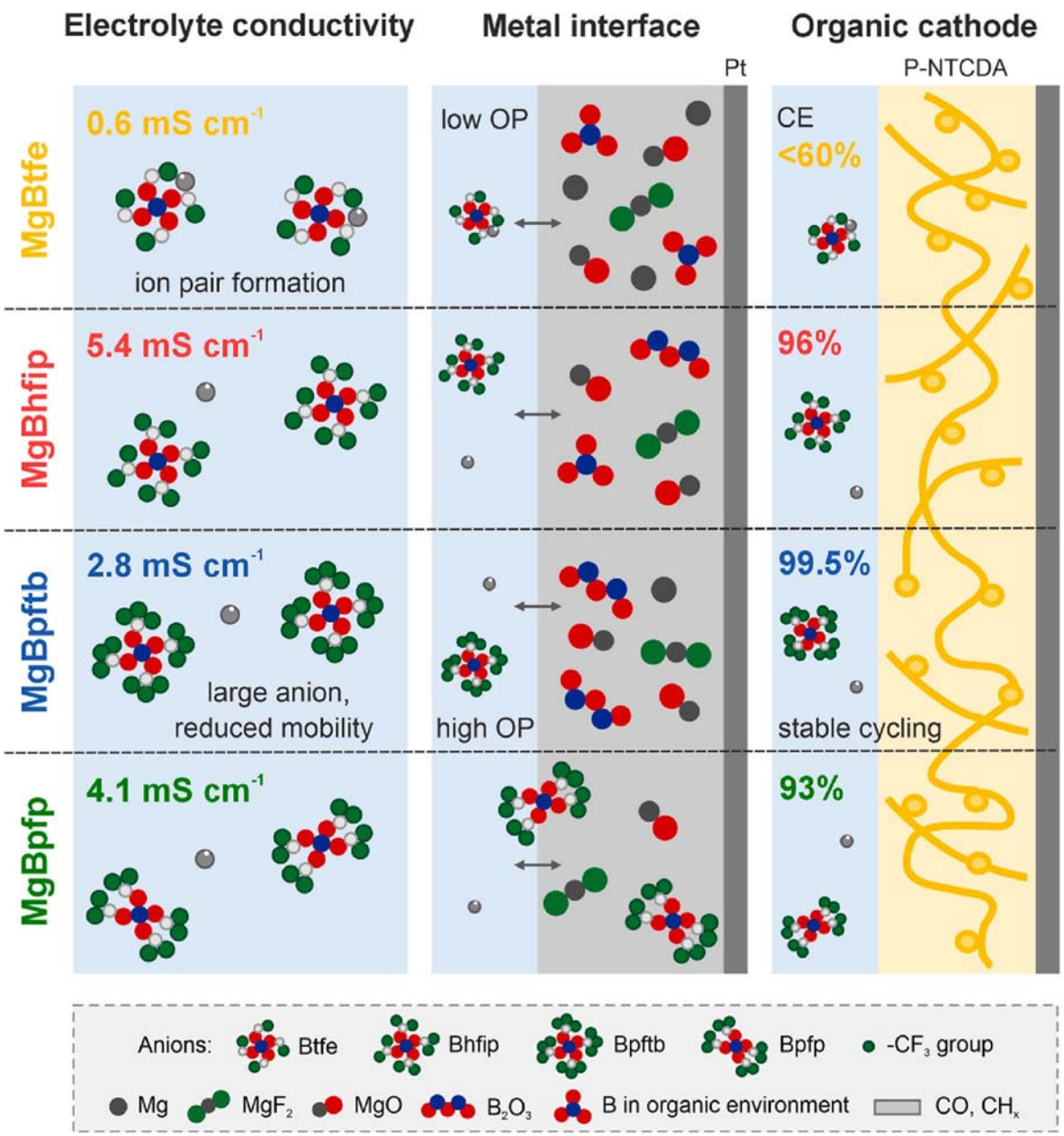

Fig. 6. Schematic representation of selected properties of fluorinated Mg alkoxyborate electrolytes: ionic conductivity, composition of the metal-electrolyte interface, and performance with the organic cathode.

3.4. Performance with the organic cathode

In the last part, we evaluated the performance of different alkoxyborate electrolytes in combination with organic cathode material based on polyimide incorporating naphthalene diimide redox active group (P-NTCDA), which shows good reversibility and cycling stability in Li electrolyte (Fig. S15). Initial electrochemical testing in Mg cells revealed poor performance of MgBpftb and MgBtfe electrolytes (Fig. 5). While in the case of MgBpftb, it was due to higher Mg plating/stripping overpotential, it was in the case of MgBtfe caused by extensive side reactions leading to average Coulombic efficiency well below 60 %. This finding is in sharp contrast with the computational modeling of Mg salts, which typically displays increased oxidative stability of MgA^+ ion pairs compared to free anions [26]. The nature of the irreversible redox processes at play in full cells remains to be elucidated. By extending the upper voltage window due to a larger overpotential in MgBpftb, we were able to increase the capacity utilization and at the same time retained good Coulombic efficiency around 99.5 % throughout the cycling. The exceptional electrochemical performance of MgBpftb in terms of cycling stability and efficiency suggests a potential move from the established MgBhfip salt to $Bpftb^-$ with a higher fluorination degree. This is especially important for testing of new generation of Mg cathodes with higher redox potentials, which are necessary next step in the development of Mg battery technology. Nevertheless, the high Mg plating/stripping overpotential of MgBpftb electrolyte should be further optimized by tuning the Mg metal interphase, either by solvent and salt concentration variation or the introduction of solvation additives [27, 28].

4. Summary and outlook

In the present work, we investigate a series of Mg alkoxyborates electrolytes with varying degrees of anion fluorination. Our findings highlight the complexity of electrolyte selection for Mg full cells in

which a compromise needs to be made between the electrolyte bulk physicochemical properties, anode, and cathode electrochemical performances, and interface stability and low resistivity. The results demonstrate the specific characteristics of different salts, and the promising electrochemical performance of alkoxyborate electrolytes, governed by different interplaying phenomena. Interestingly, despite low ionic conductivity below 1 mS cm^{-1}, the least fluorinated MgBtfe electrolyte enables Mg plating/stripping with an efficiency of nearly 99 % at 1 mA cm^{-2} and moderate overpotentials. The variation in fluorinated alkoxy ligands on the borate anion leads to different interphase layers on Mg metal deposits. While a high concentration of boron-containing species (as seen in MgBpftb and MgBtfe) increases Mg plating/stripping efficiency, the interfacial layer dominated by inorganic boron species (MgBpftb) results in significantly larger overpotentials compared to those dominated by organic boron species (MgBtfe).

Overall, the perfluorinated MgBpftb electrolyte was found to present the best combination of properties, including well-dissociated salt in solution, yet lower free anion mobility due to its larger size, a boron-rich passivation layer on the anode side and exceptional long-term capacity retention and high cycling efficiency against organic cathode (Fig. 6). However, reducing the high interfacial resistance of the MgBpftb electrolyte remains a pressing issue, and increasing the amount of organic boron species, as seen in the MgBtfe electrolyte, seems to be a promising direction. Another key insight is that high reductive stability, traditionally prioritized in Mg-based electrolyte design, may not be essential. Instead, boron-containing surface layers could prevent electrolyte reduction while enabling efficient Mg plating/stripping, potentially shifting the paradigm in electrolyte design. We believe combining these new approaches will advance the development of Mg electrolytes, bringing us toward the 99.95 % plating/stripping efficiency required for practical applications.

CRediT authorship contribution statement

Tjaša Pavčnik: Writing – review & editing, Writing – original draft, Investigation, Conceptualization. **Muath Radi:** Writing – review & editing, Writing – original draft, Investigation. **Olivera Lužanin:** Writing – review & editing, Writing – original draft, Investigation. **Rémi Dedryvère:** Writing – review & editing, Writing – original draft. **Deyana S. Tchitchekova:** Writing – review & editing, Writing – original draft, Investigation. **Alexandre Ponrouch:** Writing – review & editing, Writing – original draft, Conceptualization. **Jan Bitenc:** Writing – review & editing, Writing – original draft, Investigation, Conceptualization. **Robert Dominko:** Writing – review & editing, Writing – original draft.

Declaration of competing interest

The authors declare that they have no known competing financial interests or personal relationships that could have appeared to influence the work reported in this paper.

Acknowledgments

T. P., O. L., J. B., and R. Dominko would like to acknowledge the financial support of the Slovenian Research and Innovation Agency (ARIS) through research program P2-0423, as well as projects N2-0279 and J-4462. A.P. gratefully acknowledges funding from the European Research Council (ERC) under the European Union's Horizon 2020 research and innovation programme (grant agreement No. 101089281). A. P. and D. S. T. acknowledge the Spanish Agencia Estatal de Investigación Severo Ochoa Programme for Centres of Excellence in R&D (CEX2023-001263). M. R. acknowledges the European Union H2020-MSCA-COFUND Program for grant agreement #945357 (DESTINY project). R. Dedryvère acknowledges the French National Research Agency (ANR) for its support through the Labex STORE-EX project (ANR-10LABX-76-01).

Appendix A. Supplementary data

Supplementary data to this article can be found online at https://doi.org/10.1016/j.jpowsour.2024.235711.

Data availability

Data will be made available on request.

References

[1] S. Bobba, S. Carrara, J. Huisman, F. Mathieux, C. Pavel, . European Commission, Directorate-General for Internal Market, Industry, Critical raw materials for strategic technologies and sectors in the EU - a foresight study. https://doi.org/10.2873/58081, 2020.
[2] T. Pavčnik, M. Lozinšek, K. Pirnat, A. Vizintin, T. Mandai, D. Aurbach, R. Dominko, J. Bitenc, On the practical applications of the magnesium fluorinated alkoxyaluminate electrolyte in Mg battery cells, ACS Appl. Mater. Interfaces 14 (2022) 26766–26774, https://doi.org/10.1021/acsami.2c05141.
[3] Z. Zhao-Karger, M.E. Gil Bardaji, O. Fuhr, M. Fichtner, A new class of non-corrosive, highly efficient electrolytes for rechargeable magnesium batteries, J Mater Chem A Mater 5 (2017) 10815–10820, https://doi.org/10.1039/c7ta02237a.
[4] T. Mandai, Critical issues of fluorinated alkoxyborate-based electrolytes in magnesium battery applications, ACS Appl. Mater. Interfaces 12 (2020) 39135–39144, https://doi.org/10.1021/acsami.0c09948.
[5] Z. Li, T. Diemant, Z. Meng, Y. Xiu, A. Reupert, L. Wang, M. Fichtner, Z. Zhao-Karger, Establishing a stable anode–electrolyte interface in Mg batteries by electrolyte additive, ACS Appl. Mater. Interfaces 13 (2021) 33123–33132, https://doi.org/10.1021/acsami.1c08476.
[6] J. Luo, Y. Bi, L. Zhang, X. Zhang, T.L. Liu, A stable, non-corrosive perfluorinated pinacolatoborate Mg electrolyte for rechargeable Mg batteries, Angewandte Chemie - International Edition 58 (2019) 6967–6971, https://doi.org/10.1002/anie.201902009.
[7] T. Pavčnik, J. Bitenc, K. Pirnat, R. Dominko, Electrochemical performance of Mg metal-quinone battery in chloride-free electrolyte, Batter Supercaps 4 (2021) 815–822, https://doi.org/10.1002/batt.202000293.
[8] W. Ren, D. Wu, Y. Nuli, D. Zhang, Y. Yang, Y. Wang, J. Yang, J. Wang, An efficient bulky $Mg[B(Otfe)_4]_2$ electrolyte and its derivatively general design strategy for rechargeable magnesium batteries, ACS Energy Lett. 14 (2021) 3212–3220, https://doi.org/10.1021/acsenergylett.1c01411.
[9] P. Jankowski, Z. Li, Z. Zhao-Karger, T. Diemant, M. Fichtner, T. Vegge, J.M. G. Lastra, Development of magnesium borate electrolytes: explaining the success of $Mg[B(hfip)_4]_2$ salt, Energy Storage Mater. 45 (2022) 1133–1143, https://doi.org/10.1016/j.ensm.2021.11.012.
[10] X. Xie, N.J. Leon, D.W. Small, E.W.C. Spotte-Smith, C. Liao, K.A. Persson, Reductive decomposition kinetics and thermodynamics that govern the design of fluorinated alkoxyaluminate/borate salts for Mg-ion and Ca-ion batteries, J. Phys. Chem. C 126 (2022) 20773–20785, https://doi.org/10.1021/acs.jpcc.2c06653.
[11] A. Kopač Lautar, J. Bitenc, T. Rejec, R. Dominko, J.-S. Filhol, M.-L. Doublet, Electrolyte reactivity in the double layer in Mg batteries: an interface potential-dependent DFT study, J. Am. Chem. Soc. 142 (2020) 5146–5153, https://doi.org/10.1021/jacs.9b12474.
[12] S. Li, J. Zhang, S. Zhang, Q. Liu, H. Cheng, L. Fan, W. Zhang, X. Wang, Q. Wu, Y. Lu, Cation replacement method enables high-performance electrolytes for multivalent metal batteries, Nat. Energy 9 (2024) 285–297, https://doi.org/10.1038/s41560-023-01439-w.
[13] T. Pavčnik, J. Imperl, M. Kolar, R. Dominko, J. Bitenc, Evaluating the synthesis of $Mg[Al(hfip)_4]_2$ electrolyte for Mg rechargeable batteries: purity, electrochemical performance and costs, J Mater Chem A Mater 12 (2024) 3386–3397, https://doi.org/10.1039/d3ta06378j.
[14] Z. Zhao-Karger, R. Liu, W. Dai, Z. Li, T. Diemant, B.P. Vinayan, C. Bonatto Minella, X. Yu, A. Manthiram, R.J. Behm, M. Ruben, M. Fichtner, Toward highly reversible magnesium-sulfur batteries with efficient and practical $Mg[B(hfip)_4]_2$ electrolyte, ACS Energy Lett. 3 (2018) 2005–2013, https://doi.org/10.1021/acsenergylett.8b01061.
[15] F. Neese, The ORCA program system, Wiley Interdiscip. Rev. Comput. Mol. Sci. 2 (2012) 73–78, https://doi.org/10.1002/wcms.81.
[16] F. Weigend, R. Ahlrichs, Balanced basis sets of split valence, triple zeta valence and quadruple zeta valence quality for H to Rn: design and assessment of accuracy, Phys. Chem. Chem. Phys. 7 (2005) 3297–3305, https://doi.org/10.1039/b508541a.
[17] Socrates George, Infrared and Raman Characteristic Group Frequencies (Tables and Charts), third ed., John Wiley & Sons, 2001.
[18] A. Roy, V. Bhagavathi Parambath, T. Diemant, G. Neusser, C. Kranz, R.J. Behm, Z. Li, Z. Zhao-Karger, M. Fichtner, Investigation of the anode-electrolyte interface in a magnesium full-cell with fluorinated alkoxyborate-based electrolyte, Batter Supercaps 5 (2022) e202100305, https://doi.org/10.1002/batt.202100305.

[19] T. Mandai, Y. Youn, Y. Tateyama, Remarkable electrochemical and ion-transport characteristics of magnesium-fluorinated alkoxyaluminate–diglyme electrolytes for magnesium batteries, Mater Adv 2 (2021) 6283–6296, https://doi.org/10.1039/d1ma00448d.

[20] D. Samuel, C. Steinhauser, J.G. Smith, A. Kaufman, M.D. Radin, J. Naruse, H. Hiramatsu, D.J. Siegel, Ion pairing and diffusion in magnesium electrolytes based on magnesium borohydride, ACS Appl. Mater. Interfaces 9 (2017) 43755–43766, https://doi.org/10.1021/acsami.7b15547.

[21] J. Barthel, H.J. Gores, G. Schmeer, The temperature dependence of the properties of electrolyte solutions. III. Conductance of various salts at high concentrations in propylene carbonate at temperatures from − 45°C to + 25°C, Ber. Bunsen Ges. Phys. Chem. 83 (1979) 911–920, https://doi.org/10.1002/bbpc.19790830908.

[22] T. Mandai, K. Yoshida, S. Tsuzuki, R. Nozawa, H. Masu, K. Ueno, K. Dokko, M. Watanabe, Effect of ionic size on solvate stability of glyme-based solvate ionic liquids, J. Phys. Chem. B 119 (2015) 1523–1534, https://doi.org/10.1021/jp508100s.

[23] Y. Yamada, K. Furukawa, K. Sodeyama, K. Kikuchi, M. Yaegashi, Y. Tateyama, A. Yamada, Unusual stability of acetonitrile-based superconcentrated electrolytes for fast-charging lithium-ion batteries, J. Am. Chem. Soc. 136 (2014) 5039–5046, https://doi.org/10.1021/ja412807w.

[24] J.F. Moulder, W.F. Stickle, P.E. Sobol, K.D. Bomben, Handbook of X-ray photoelectron spectroscopy: a reference book of standard spectra for identification and interpretation of XPS data, in: Physical Electronics Division, Perkin-Elmer Corporation, Eden Praire, Minnesota, USA, 1992.

[25] J. Forero-Saboya, C. Davoisne, R. Dedryvère, I. Yousef, P. Canepa, A. Ponrouch, Understanding the nature of the passivation layer enabling reversible calcium plating, Energy Environ. Sci. 13 (2020) 3423–3431, https://doi.org/10.1039/d0ee02347g.

[26] K.-C. Lau, T.J. Seguin, E.V. Carino, N.T. Hahn, J.G. Connell, B.J. Ingram, K. A. Persson, K.R. Zavadil, C. Liao, Widening electrochemical window of Mg salt by weakly coordinating perfluoroalkoxyaluminate anion for Mg battery electrolyte, J. Electrochem. Soc. 166 (2019) A1510–A1519, https://doi.org/10.1149/2.0751908jes.

[27] S. Hou, X. Ji, K. Gaskell, P. Wang, L. Wang, J. Xu, R. Sun, O. Borodin, C. Wang, Solvation sheath reorganization enables divalent metal batteries with fast interfacial charge transfer kinetics, Science 374 (2021) (1979) 172–178, https://doi.org/10.1126/science.abg3954.

[28] C. Li, R.D. Guha, A. Shyamsunder, K.A. Persson, L.F. Nazar, A weakly ion pairing electrolyte designed for high voltage magnesium batteries, Energy Environ. Sci. 17 (2024) 190–201, https://doi.org/10.1039/d3ee02861e.